Eur. Phys. J. E (2015) **38**: 38
DOI 10.1140/epje/i2015-15038-y

THE EUROPEAN PHYSICAL JOURNAL E

Regular Article

Numerical investigation of thermo-magneto-solutal flow of ferrocolloid through ordered and disordered permeable membranes*

Dmitry Zablotsky[a] and Elmars Blums

Institute of Physics, Latvian University, Miera str. 32, Salaspils-1 LV-2169, Latvia

Received 16 July 2014 and Received in final form 10 March 2015
Published online: 15 May 2015 –

Abstract. We explore the mechanism of ferroparticle transfer in porous structures in the conditions of simultaneous action of the thermal gradient and the magnetic field. We show that when a ferrocolloid saturated porous matrix is placed in a homogeneous magnetic field the grains of the porous frame notably distort the uniformity of the internal field by creating sharp gradients in the vicinity of the interface. On the other hand, the application of the temperature gradient creates an imbalance of the ferroparticle concentration in the bulk of the porous structure due to colloidal thermophoresis. The combination of the imbalance of concentration of the magnetic nanoparticles and the internal gradients of the magnetic field creates a magnetic force and convective flow of solution through the porous structure. We report the results of the pore-scale numerical simulations of the ferrocolloid thermo-magneto-solutal flow in geometrically simple ordered and disordered permeable structures and membranes with different porosity.

1 Introduction

Ferrocolloids are stabilized colloidal solutions, which consist of magnetic nanoparticles suspended in a liquid carrier. These binary systems display pronounced colloidal thermophoresis (Soret effect) [1,2], *i.e.* the presence of a temperature gradient in a sample of ferrocolloid leads to the establishing of the corresponding concentration gradient of the suspended nanoparticles. The magnitude of the thermophoretic separation is determined by the value of the Soret coefficent. In ferrocolloids its typical values are two to three orders of magnitude larger than in molecular mixtures $S_T \approx \pm 0.1 \ldots 0.16\,\mathrm{K}^{-1}$ and depending on the composition of the colloid its sign can be positive or negative corresponding to normal or anomalous thermophoresis [3,4], *i.e.* establishing of the concentration gradient in the direction of the temperature gradient or in the opposite direction. At the same time the diffusive mobility of the nanoparticles is very low and the dynamics of the concentration field in a ferrocolloid is significant only on submillimeter scale where the concentration profile can be established in experimentally relevant time.

As solutions of magnetic nanoparticles the ferrocolloids strongly interact with the magnetic field [5]. Even a homogeneous field can lead to the appearance of the magnetic buoyant forces. The possibility of the magnetic control over the intensity and direction of mass transport is the attracting property of these materials. Fluidic actuation, mobilization of particles and mixing are important problems on the micro-scale, especially in microfluidic applications.

While the theoretical considerations [6,7] evidence that the dependence of the thermophoretic drift on the magnetic field in the bulk of the ferrocolloid should be weak, sometimes the stratification of the ferrocolloid in a magnetic field can be accompanied by the magnetically driven microconvective processes [8–15], which intensify the internal mixing and lead to a considerable attenuation of the established concentration gradient.

The experimental investigations show a significant dependence of the ferroparticle Soret coefficient on the magnetic field [16]. Some recent experiments on the thermophoretic separation of the ferrocolloid through permeable membranes [17–19] have demonstrated a considerable decrease of the measured Soret coefficient and enhanced mixing due to the applied magnetic field. A similar effect was observed also in porous layers [20]. The microscopic mechanism of these phenomena is not sufficiently understood at the moment. The advective mass transport can lead to the enhanced mixing and attenuation of the thermophoretic separation in ferrocolloid saturated permeable structures [21]. The possibility of the presence of the magnetic microconvection, which is created by the complex simultaneous interaction of the thermal gradient,

* Contribution to the Topical Issue "Thermal non-equilibrium phenomena in multi-component fluids" edited by Fabrizio Croccolo and Henri Bataller.

[a] e-mail: Dmitrijs.Zablockis@gmail.com

ferroparticle concentration and external magnetic field, in these media cannot be excluded.

When a system of non-magnetic inclusions is immersed in ferrocolloid and placed in the external homogeneous magnetic field the magnetic colloid becomes magnetized and a discontinuity of the magnetization appears across the surface of the non-magnetic inclusions. The inclusion creates a perturbation of the external field and large gradients of the magnetic field may appear in the vicinity of its surface. The gradient of the magnetic field leads to the appearance of the magnetic force acting on the magnetic colloid. In isothermal homogeneous ferrocolloid this force is potential and is not capable of inducing a sustained convective motion. On the other hand, if a temperature gradient persists within the magnetic colloid simultaneously with the external magnetic field it induces the formation of the corresponding gradient of the ferroparticle concentration due to the strong colloidal thermophoresis. The magnetization of the ferrocolloid strongly depends on the concentration of the magnetic particles. In a non-homogeneous ferrocolloid the magnetic force becomes non-potential and the magnetic convection may emerge as the result.

At submillimeter scale the leading role in driving the convective motion is assumed by the concentration of the magnetic solute. The dependence of the ferrocolloid magnetization on the temperature itself is much weaker and becomes important only on larger length scales. Therefore, the relevant mechanism of the magnetic buoyancy is magnetosolutal.

Here we consider porous structures and membranes as such systems of non-magnetic inclusions immersed in a magnetic colloid. The presence of the internal magnetic microconvection may explain the unusual enhancement of mixing in the porous layers and membranes.

2 Governing equations

2.1 Pore-scale equations

The magnetic force acting on the magnetized ferrocolloid in the presence of a non-homogeneous magnetic fields $\mathbf{F} = \mu_0(\mathbf{M}\nabla)\mathbf{H}$ [22]. In equilibrium the magnetization of the ferrocolloid $\mathbf{M} = \chi(c, H)\mathbf{H}$. Its magnetic susceptibility χ depends on the concentration of the ferroparticles and the magnetic field. Assuming non-interacting ferroparticles the linear relation holds $\chi(c, H) = \chi_0(1 + \chi_c \Delta c)$ for the dependence of the magnetic susceptibility on concentration, where $\Delta c = c - c_0$ is the deviation of the concentration from the reference value c_0, χ_0 is the magnetic susceptibility of the ferrocolloid at reference concentration and magnetic field and $\chi_c = \frac{1}{\chi_0}\frac{\partial \chi}{\partial c} = \frac{1}{c_0}$ is the expansion coefficient.

We introduce the characteristic scales: characteristic length R_0, mass transfer Fourier number $Fo_m = DR_0^{-2}$ as time scale $\tilde{t} = Fo_m t$ (here D is the diffusion coefficient of the ferroparticles), $\overline{\Delta H}$ for the magnetic field and $\overline{\Delta c}$ for the concentration.

The non-potential part of the magnetic force acting on the non-homogeneous ferrocolloid then can be written in a dimensionless form

$$\mathbf{F} = Rs_m c \nabla \left[(\mathbf{h} + r_H \delta\mathbf{H})\, \delta\mathbf{H} \right], \tag{1}$$

where $\mathbf{h}$ is the unit vector in the direction of the reference magnetic field $\mathbf{H_0}$, $\delta\mathbf{H} = (\overline{\Delta H})^{-1}(\mathbf{H} - \mathbf{H_0})$ is the deviation of the magnetic field from the reference, $c = (\overline{\Delta c})^{-1}\Delta c$ is the normalized perturbation of the ferroparticle concentration and the coefficient $r_H = \frac{1}{2}H_0^{-1}\overline{\Delta H}$ determines the relative magnitude of the magnetic field perturbation in relation to the reference field. The value of the parameter r_H is usually less than 5% so this contribution is neglected.

From (1) it follows that indeed the simultaneous presence of the variations of the concentration and magnetic field perturbations in the bulk of the ferrocolloid can produce convective motion. By analogy with the solutal buoyancy in conventional mixtures this mechanism of magnetic buoyancy is magnetosolutal and is present only in the magnetic colloids.

The dimensionless parameter Rs_m is the magnetosolutal Rayleigh number

$$Rs_m = \mu_0 \chi_0 \chi_c H_0 \frac{L^2}{\eta D} \overline{\Delta c \Delta H}, \tag{2}$$

which characterizes the relative strength of the magnetosolutal buoyant effect.

Assuming that a non-magnetic cylindrical inclusion is immersed in a magnetized isothermal homogeneous ferrofluid with magnetic permeability $\mu_r = 1 + \chi_0$ and a uniform internal magnetic field H_0, it then creates around itself a perturbation of the otherwise homogeneous magnetic field [23]. In cylindrical coordinates the dimensionless magnetic perturbation:

$$\delta\mathbf{H}(r, \theta) = -\frac{\cos\theta}{r^2}\mathbf{e_r} - \frac{\sin\theta}{r^2}\mathbf{e}_\theta. \tag{3}$$

We define the characteristic length scale R_0 as the radius of the inclusion and the scale of the magnetic field then becomes $\overline{\Delta H} = K_H H_0$ with $K_H = \frac{\mu_r - 1}{\mu_r + 1}$.

The perturbation of the magnetic field in the vicinity of the non-magnetic cylindrical inclusion is illustrated in fig. 1. Due to the presence of a discontinuity of the magnetization, the magnetic field is highly non-homogeneous and possesses rather sharp gradients near the surface of the inclusion. The gradients of the magnetic field may contribute to the appearance of non-potential magnetic forces in a non-homogeneous ferrocolloid (1) leading to the emergence of the magnetosolutal flow. The complex structure of the magnetic field around the inclusion (fig. 1) may promote different kinds of magnetosolutal flow—the mixing component corresponds to the internal convective circulations within the individual pores and integral flow of the ferrocolloid across the non-magnetic inclusion is possible as well [24,25].

The linearized mass flux of the ferroparticles in non-homogeneous and non-isothermal ferrocolloids contains

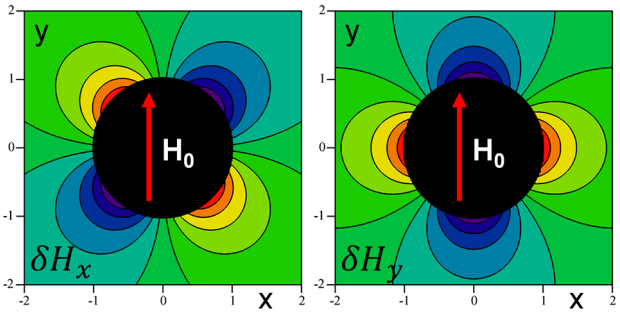

Fig. 1. Perturbation $\delta\mathbf{H}$ of the internal homogeneous magnetic field $\mathbf{H_0}$ in a ferrocolloid introduced by the non-magnetic cylindrical inclusion: left: x-component of magnetic perturbation; right: y-component.

principal contributions from advection, gradient diffusion and thermophoretic separation due to a temperature gradient ∇T [22]

$$\mathbf{J} = \mathbf{u}c - D\nabla c - c_0(1-c_0)DS_T\nabla T. \tag{4}$$

Here we have purposefully neglected the magnetophoretic contribution to the mass flux, which could be important in the immediate vicinity of the non-magnetic inclusions due to the presence of the gradients of the magnetic field there. This is done to avoid introducing additional effects and to keep the problem as simple as possible.

The characteristic scale for the deviation of the ferroparticle concentration can now be defined in terms of the applied temperature gradient as $\overline{\Delta c} = c_0(1-c_0)S_T R_0|\nabla T|$.

Based on (4) the evolution of the ferroparticle concentration is governed by the basic advection-diffusion equation in dimensionless form

$$\frac{\partial c}{\partial t} + \mathbf{u}\nabla c = \Delta(c+T). \tag{5}$$

The Lewis number $Le = \frac{D}{\alpha}$, defined as a ratio of the mass diffusivity D and thermal diffusivity α determines the difference in time scales between the processes of the mass and heat transfer. Owing to the low mobility of the nanoparticles in colloidal solutions the characteristic value of the Lewis number in ferrocolloids is very small $Le \sim 10^{-3}$. Thus, the magnetosolutal flows described by the diffusion time scale are not capable of influencing the distribution of the temperature. We then neglect the advection of the temperature field.

In turn, the Schmidt number $Sc = \frac{\eta}{\rho D}$, which describes the ratio of the momentum and mass diffusivities, is very large (of the order $\sim 10^4$–10^5) in ferrocolloids. Here we consider the systems with a characteristic size on the submillimeter scale. Consequently, the magnetosolutal flow is completely dominated by the momentum diffusion.

For the description of the creeping flow in the porous structures we introduce the Stokes equation, in dimensionless form

$$-\nabla p + \Delta u + \mathbf{F} = 0 \tag{6}$$

along with the flow continuity condition $\nabla \cdot \mathbf{u} = 0$.

For the characteristic parameters of the ferrocolloid, the Soret coefficient $S_T = 0.1\,\mathrm{K}^{-1}$, the dynamic viscosity is $\eta = 0.001\,\mathrm{Pa\,s}$, the mass concentration of ferroparticles is $c_0 = 0.15$, the particle diameter is $d = 8\,\mathrm{nm}$, the diffusion coefficient is $D = 2\cdot 10^{-11}\,\mathrm{m\,s^{-2}}$, the spontaneous magnetization of the ferromagnetic material is $M_S = 5\cdot 10^5\,\mathrm{A\,m^{-1}}$ and in the presence of the magnetic field of 0.1 T and the thermal gradient of 20 K over a distance of 1 mm applied simultaneously across a cylindrical inclusion with the radius 2 μm, the magnetosolutal Rayleigh number in the vicinity of the inclusion reaches $Rs_m \sim 50$. It is reasonable then to suspect the presence of the magnetosolutal flow within a porous structure in these circumstances.

2.2 Darcy scale

The real porous structures often contain a large number of solid grains. It is then numerically complicated and usually even unnecessary to resolve the pore-scale transport in large systems. In the macroscopic porous structures the resolution of the macro-scale transport is usually required while the peculiarities of the micro-scale processes are accommodated through the appropriate physical models and modeling parameters. The macroscopic models of the heterogeneous media can be obtained by volume averaging of the pore-scale equations [26] and written in terms of the macroscopic spatial averages.

The averaging of the Stokes equation (6) yields the Darcy equation [27]

$$\epsilon\langle\mathbf{u}\rangle^\beta = -Da\left(\nabla\langle p\rangle^\beta - \langle\mathbf{F}\rangle^\beta\right), \tag{7}$$

accompanied by the continuity condition $\nabla\cdot\langle\mathbf{u}\rangle^\beta = 0$ and written in terms of the intrinsic averages $\langle\,\rangle^\beta$, *i.e.* averages over the fluid part of the averaging volume. The parameter $\epsilon = V^\beta/V$ is the porosity of the porous medium. It determines the part of the total averaging volume V occupied by the fluid phase V^β.

The dimensionless Darcy number $Da = KR_0^{-2}$ in eq. (7) introduces the hydraulic permeability K of the porous structure, which is the property of the geometry of the porous matrix and can be calculated by several methods: the Kozeny-Carman equations [28] and similar analytic correlations [29] or as the solution of the closure problem. We use the latter method described in [26].

In turn, the dimensionless averaged advection-diffusion equation in the simplest form for a porous medium with uniform porosity and neglecting the terms corresponding to the interfacial transport and dispersion of the solute concentration becomes [30]

$$\frac{\partial\langle c\rangle^\beta}{\partial t} + \langle\mathbf{u}\rangle^\beta\nabla\langle c\rangle^\beta = \Delta\left(\langle c\rangle^\beta + \langle T\rangle^\beta\right). \tag{8}$$

Written in terms of the intrinsic averages, it is similar in form to its pore-scale counterpart (5).

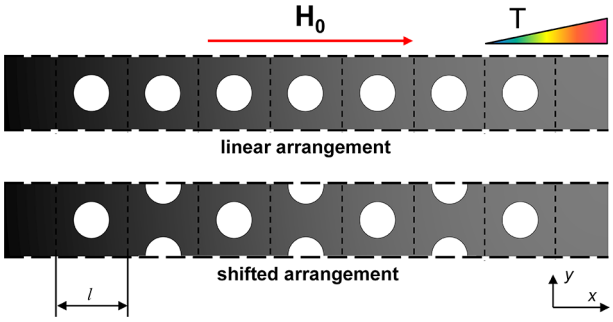

Fig. 2. Considered ordered geometries of the porous membranes: top: linear arrangement; bottom: shifted arrangement.

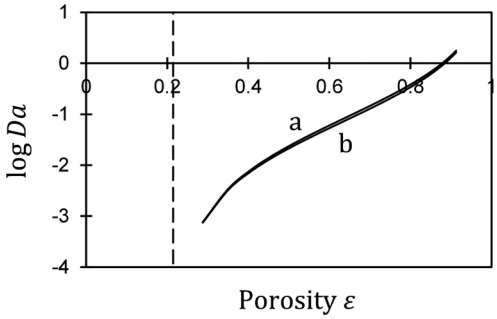

Fig. 3. Calculated dependence of the Darcy number on the membrane porosity for the ordered porous structures: (a) linear arrangement, (b) shifted arrangement.

3 Ordered porous structures

As the models of porous media we assume the arrangements of cylindrical elements, which represent the grains of the porous structure and form systems with different geometries. Two types of systems are considered: a) ordered geometries, which are spatially periodic and possess a corresponding unit cell and a set of the lattice vectors; b) disordered geometries, for which no unit cell can be defined [26].

We investigate two kinds of ordered porous media. One arrangement is a periodic 1D system of cylinders spaced equidistantly along a common axis (fig. 2). The corresponding unit cell consists of a square fluid domain with the side length l and a solid circular inclusion of a unit radius placed in the center of it.

The other arrangement is similar but every even cylinder is shifted by a half of the period in the y-direction (fig. 2). We note that the total number of elements in both cases is chosen to be odd so that the surface of the membrane would be identical on either side for both arrangements. We call the first arrangement a linear arrangement and the second a shifted arrangement. The number of the elements composing the membrane is also sufficiently large so that the properties of the flow in either case would not depend on the size of the membrane.

The macroscopic hydraulic properties of the membrane are determined by its Darcy number $Da(\epsilon)$, which is a function of the porosity ϵ. The porosity of the membrane is identical for both the linear and the shifted arrangement and can be calculated from a simple relation $\epsilon = 1 - \pi l^{-2}$. We can adjust the porosity in the interval from ~ 0.215, which is the minimum value for these arrangements, up to ~ 1 by changing the size l of the unit cell.

We calculate the hydraulic permeability (and the corresponding Darcy number) of the membrane numerically by solving the closure problem within a unit cell of the ordered membrane with periodic boundary conditions in x- and y-directions as detailed in [26].

The dependence of the Darcy number on the porosity for both ordered arrangements is shown in fig. 3. Because the shifted arrangement is slightly anisotropic the component of the permeability tensor in the x-direction is taken in this case. The calculations show a close match between the corresponding values of the Darcy number for both geometries and within a wide range of the values of the porosity. The hydraulic properties of the membrane should thus be nearly identical in both cases, but the microscopic configurations of the magnetic field and the corresponding magnetic force will be different.

Assuming the specific geometry (fig. 2) we calculate the magnetosolutal flow passing through the membrane by solving the eqs. (6) and (5) numerically. The regions filled with the homogeneous fluid are created on both sides of the membrane. The length of these regions is chosen to be sufficiently large so that the free stream boundary conditions —zero gradient of velocity— could be applied on the entrance and exit of the domain in the x-direction. Symmetry boundary conditions are imposed on the sidewalls of the domain in the y-direction. The no-slip boundary conditions are assumed on the surface of the cylindrical inclusions.

A unit temperature gradient $|\nabla T| = 1$ is applied across the membrane and the homogeneous magnetic field is imposed in the same direction. We assume that the thermal conductivity of the inclusions is the same as that of the ferrocolloid and their presence does not perturb the temperature field. In response to the appearance of the thermal gradient a corresponding gradient of the ferroparticle concentration begins to form. We start all calculations from a steady thermophoretic separation $\nabla c = -\nabla T$ assuming a positive value of the Soret coefficient. The surface of the inclusions is treated as impermeable to the mass flux of the ferroparticles $\mathbf{J} \cdot \mathbf{n} = 0$ and the advective perturbation of the initial thermophoretic concentration gradient vanishes in the free stream on both sides of the membrane.

Two series of simulations are performed: in the first (case 0) we only solve the Stokes equation (6) and do not solve the advection-diffusion equation (5). This means that we neglect the advective transport of the ferroparticle concentration. This is an artificial situation, which will nevertheless be useful. In the second series of simulations (case 1) we solve the Stokes equation and the advection-diffusion equation in conjunction advancing the solution to the stationary (or quasi-stationary) state. In these calculations we take into account the advection of the ferroparticles.

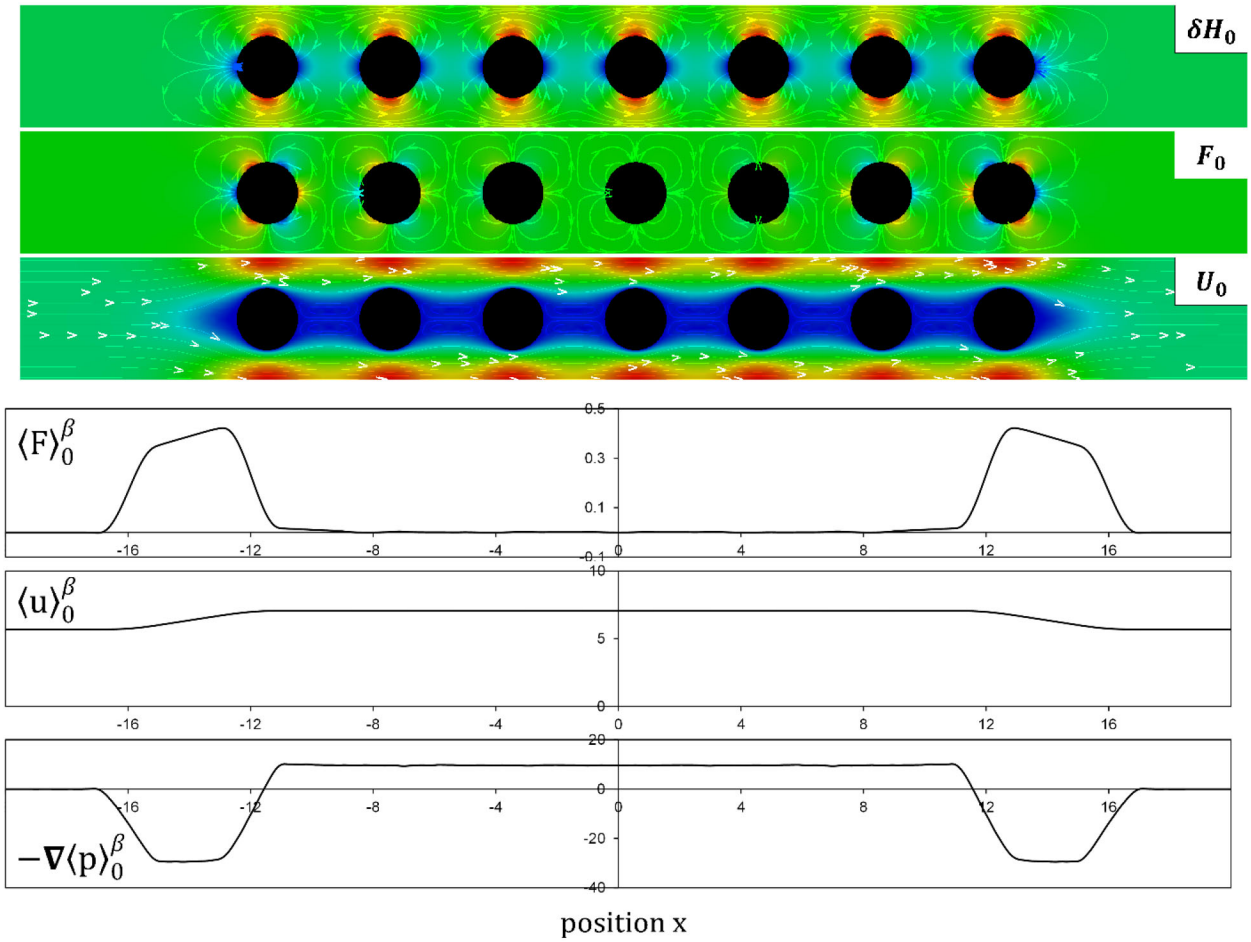

Fig. 4. Linear arrangement, series of calculations without the influence of advection (case 0): Magnetic field perturbation $\delta\mathbf{H}$ (field lines and distribution of $\mathbf{h} \cdot \delta\mathbf{H}$), magnetic force $\mathbf{F}$ (lines of force and distribution of F_x), velocity of the magnetosolutal flow $\mathbf{u}$ (streamlines and distribution of velocity magnitude), plot of averaged magnetic force $\langle \mathbf{F} \rangle^\beta$, plot of averaged velocity $\langle \mathbf{u} \rangle^\beta$, plot of the gradient of averaged pressure $-\nabla \langle p \rangle^\beta$.

3.1 Linear arrangement

The calculated perturbation of the magnetic field created by the immersed non-magnetic inclusions in the linear arrangement is illustrated in fig. 4. Imposing the initial concentration gradient $\nabla c = -\nabla T$ we calculate the corresponding distribution of the magnetic force (1) acting on the ferrocolloid. The magnetic force (fig. 4) is notably non-uniform and clearly could cause pore-scale convective circulations. In order to discard the microscopic oscillations and reveal its macroscopic structure we perform the spatial averaging. The correct average in the ordered porous media is the cellular average [26]. In order to smooth the periodic oscillations it is necessary to average the magnetic force twice across a unit cell of the periodic porous structure. Figure 4 shows the distribution of the cellular average of the magnetic force within the membrane. Thus the macroscopic magnetic force completely vanishes within the bulk of the membrane and is localized exclusively in the immediate vicinity of the membrane surface reaching a sharp maximum within approximately a single period of the porous structure. While the averaged magnetic force is well localized, its maximum value is proportional to the value of the concentration at both ends of the membrane. So, when a concentration gradient is applied across the porous membrane, the total magnetic force and subsequently the created pressure difference are proportional to the thickness of the membrane.

Next we solve the Stokes equation using the predetermined distribution of the magnetic force. The calculated distribution of the pore-scale velocity is shown in fig. 4. As expected aside from the pore-scale convective circulations the magnetosolutal buoyant forces produce notable integral flow through the porous membrane in the direction of the decreasing concentration (or increasing temperature in the case of the positive Soret effect). Due to the neighboring cylindrical elements shadowing each other from the flow the space between the inclusions is occupied by almost stagnant fluid.

The cellular average of the velocity field (fig. 4) shows that the flow is uniform within the bulk of the membrane. The value of the averaged velocity in the free stream out-

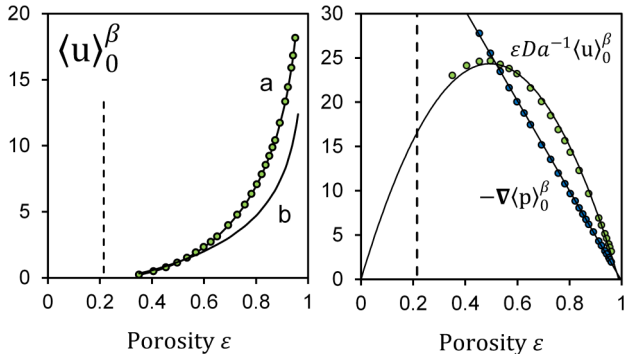

Fig. 5. Linear arrangement, series of calculations without the influence of advection (case 0). Left: dependence of averaged velocity in the bulk of the membrane on porosity: (a) pore-scale simulations; (b) predictions of Darcy's law. Right: dependence of $-\nabla\langle p\rangle^\beta$ and $\epsilon Da^{-1}\langle u\rangle^\beta$ in the bulk of the membrane on porosity calculated from pore-scale simulations.

side the membrane is proportional to the velocity in the center of the membrane and the porosity of the membrane ϵ as required by the continuity of the flow.

According to Darcy's law (7) a simple linear relationship should hold between the gradient of the averaged pressure, the magnetic force and the velocity in the bulk of the membrane. In fig. 5 we compare the values of the averaged velocity $\langle u\rangle_0^\beta$ obtained from numerical simulations of the case with the imposed concentration gradient and without the influence of advection (case 0) and the predictions of Darcy's law based on the gradient of the averaged pressure $\nabla\langle p\rangle_0^\beta$ (the cell-averaged magnetic force vanishes in the bulk of the membrane in the simulations without advection and so does the corresponding term in Darcy's equation) for different porosities. While there is a reasonable correspondence and scaling with respect to the porosity, the error can reach up to 30%.

To reveal the cause of this discrepancy we plot the dependence of the pressure gradient $-\nabla\langle p\rangle_0^\beta$ on the porosity (fig. 5) within the membrane and compare it with the calculated quantity $\epsilon Da^{-1}\langle u\rangle_0^\beta$, which has the meaning of the force density. The pressure gradient scales linearly with increasing the porosity, while the latter quantity obeys a parabolic dependence, which is the reason for the failure of Darcy's law.

In the second series of calculations (case 1) we solve the Stokes equation (6) in conjunction with the advection-diffusion equation (7) taking into account the advective transport of the ferroparticle concentration. We advance the solution in time from the initial state corresponding to the purely thermophoretic separation $\nabla c = -\nabla T$ towards the stationary state.

Since the velocity in the bulk of the membrane is higher than that in the free stream region the value of the gradient of the averaged concentration decreases within the membrane (fig. 6) due to the increased advective flux in the direction of the decreasing concentration. The magnitude of this effect can be estimated from the macro-scale equations.

Assuming that a steady flow of the ferrocolloid is passing through the membrane with the porosity ϵ and a concentration gradient $(\nabla\langle c\rangle^\beta)|_{\text{out}}$ is established in the free stream on both sides across the membrane (fig. 7), from eq. (8) it follows that within the membrane

$$\frac{\partial}{\partial t}\langle c\rangle_{\text{in}}^\beta + \langle \mathbf{u}\rangle_{\text{in}}^\beta \left(\nabla\langle c\rangle^\beta\right)\big|_{\text{in}} = 0 \tag{9}$$

and in the free stream on both sides of the membrane,

$$\frac{\partial}{\partial t}\langle c\rangle_{\text{out}}^\beta + \langle \mathbf{u}\rangle_{\text{out}}^\beta \left(\nabla\langle c\rangle^\beta\right)\big|_{\text{out}} = 0. \tag{10}$$

At the surface of the membrane (points P_1 and P_2, fig. 7) $\langle c\rangle_{\text{in}}^\beta = \langle c\rangle_{\text{out}}^\beta$. In turn, the velocity of the flow within the membrane $\langle \mathbf{u}\rangle_{\text{in}}^\beta = \epsilon^{-1}\langle \mathbf{u}\rangle_{\text{out}}^\beta$. It follows then that the magnitude of the established concentration gradient inside the membrane should be proportional to its porosity

$$\left(\nabla\langle c\rangle^\beta\right)\big|_{\text{in}} = \epsilon\left(\nabla\langle c\rangle^\beta\right)\big|_{\text{out}}. \tag{11}$$

In fig. 8 we have plotted the value of the gradient of the cell-averaged concentration $\nabla\langle c\rangle^\beta$ in the center of the membrane for different porosities. Since the magnitude of the concentration gradient in the free stream is equal to 1, the concentration gradient inside the membrane is indeed proportional to the porosity.

Advection of the ferroparticle concentration within the membrane influences the magnitude and distribution of the magnetic force (fig. 6). Due to the decrease of the concentration gradient the magnetic force becomes asymmetric with respect to the center of the membrane. Additionally, there also appears a negative component of the magnetic force in the bulk of the membrane, which opposes the pressure difference created on both surfaces of the membrane. This is not the consequence of the decreasing of the concentration gradient due to the integral flow (11), which was discussed previously. This is a microscopic effect caused by the periodic narrowing and expansion of the streamlines within the pores of the membrane resulting in pore-scale mixing. The interaction of the magnetic perturbation introduced by the non-magnetic inclusions with the perturbation of the concentration gradient by the advective circulations just within the individual pores leads to the appearance of this opposing magnetic force.

In fig. 8 we check the validity of Darcy's law (7) for the series of calculations with account for advection (case 1). In this case the averaged velocity in the bulk of the membrane $\langle u\rangle^\beta$ calculated from the pore-scale simulations is only growing with respect to the porosity up to $\epsilon \approx 0.87$ and further increasing the porosity it begins to decrease. This happens due to the interference of the vortices located in between the cylindrical inclusions (fig. 4). The prediction of the velocity calculated from the pressure gradient $\nabla\langle p\rangle^\beta$ and magnetic force $\langle \mathbf{F}\rangle^\beta$ in the center of the membrane according to Darcy's law (7) is adequate only at relatively low values of the porosity and considerably underestimates the flow velocity at larger porosity. Based on the values of the averaged velocity $\langle u\rangle_0^\beta$ calculated in

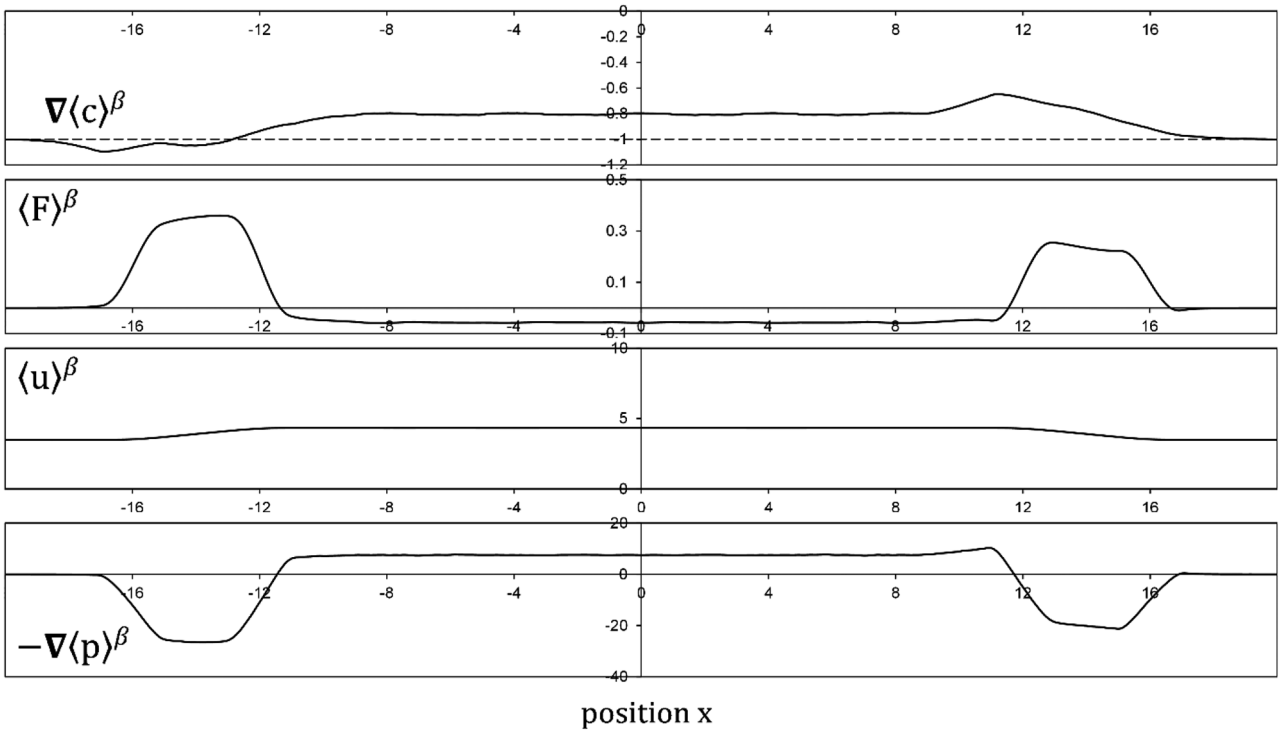

Fig. 6. Linear arrangement, calculations with account for advection (case 1): plot of the gradient of averaged concentration $\nabla\langle c\rangle^{\beta}$, plot of averaged magnetic force $\langle\mathbf{F}\rangle^{\beta}$, plot of averaged velocity $\langle\mathbf{u}\rangle^{\beta}$, plot of the gradient of averaged pressure $-\nabla\langle p\rangle^{\beta}$.

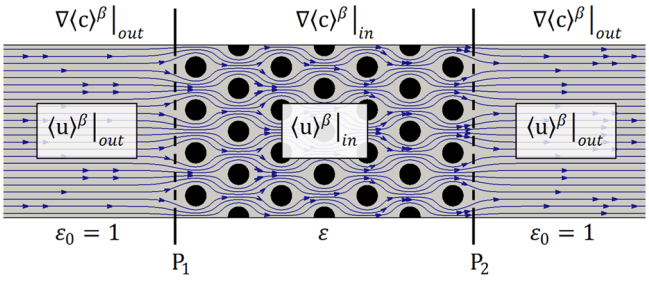

Fig. 7. Magnetosolutal flow through a permeable membrane with porosity ϵ and associated macroscopic quantities: averaged velocity $\langle\mathbf{u}\rangle^{\beta}_{\mathrm{in}}$ and ferroparticle concentration gradient $\nabla\langle c\rangle^{\beta}|_{\mathrm{in}}$ inside the membrane and $\langle\mathbf{u}\rangle^{\beta}_{\mathrm{out}}$, $\nabla\langle c\rangle^{\beta}|_{\mathrm{out}}$ in the free stream.

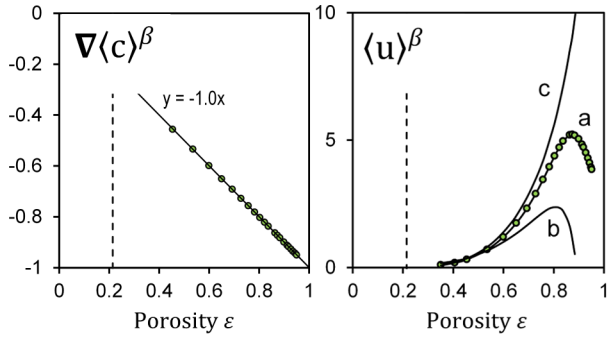

Fig. 8. Linear arrangement, calculations with account for advection (case 1). Left: dependence of the gradient of concentration in the bulk of the membrane on porosity calculated from pore-scale simulations. Right: dependence of the averaged velocity in the bulk of the membrane on porosity: (a) pore-scale simulations, (b) predictions of Darcy law, (c) empirical correlation $\epsilon\langle u\rangle^{\beta}_{0}$ where $\langle u\rangle^{\beta}_{0}$ is the corresponding velocity calculated from simulations without the influence of advection (case 0).

the series of simulations without account for advection (case 0) an empirical correlation can be used,

$$\langle u\rangle^{\beta} = \epsilon\langle u\rangle^{\beta}_{0}, \tag{12}$$

to estimate the averaged velocity $\langle u\rangle^{\beta}$ in the bulk of the membrane with the influence of advection (case 1). The correspondence of this empirical relation with the results of the case 1 simulations (fig. 8) is good up to the point where the flow structure begins to change leading to the decrease of the averaged velocity with the growing porosity. The obvious but useful conclusion is that the averaged velocity $\langle u\rangle^{\beta}$ is proportional to the gradient of concentration within the membrane. As previously discussed, advection causes the decrease of the concentration gradient in the bulk of the membrane proportionally to the value of its porosity (11) (at unit concentration gradient in the free stream) and it appears that the velocity decreases in the same proportion in the calculations with account for the advective transport.

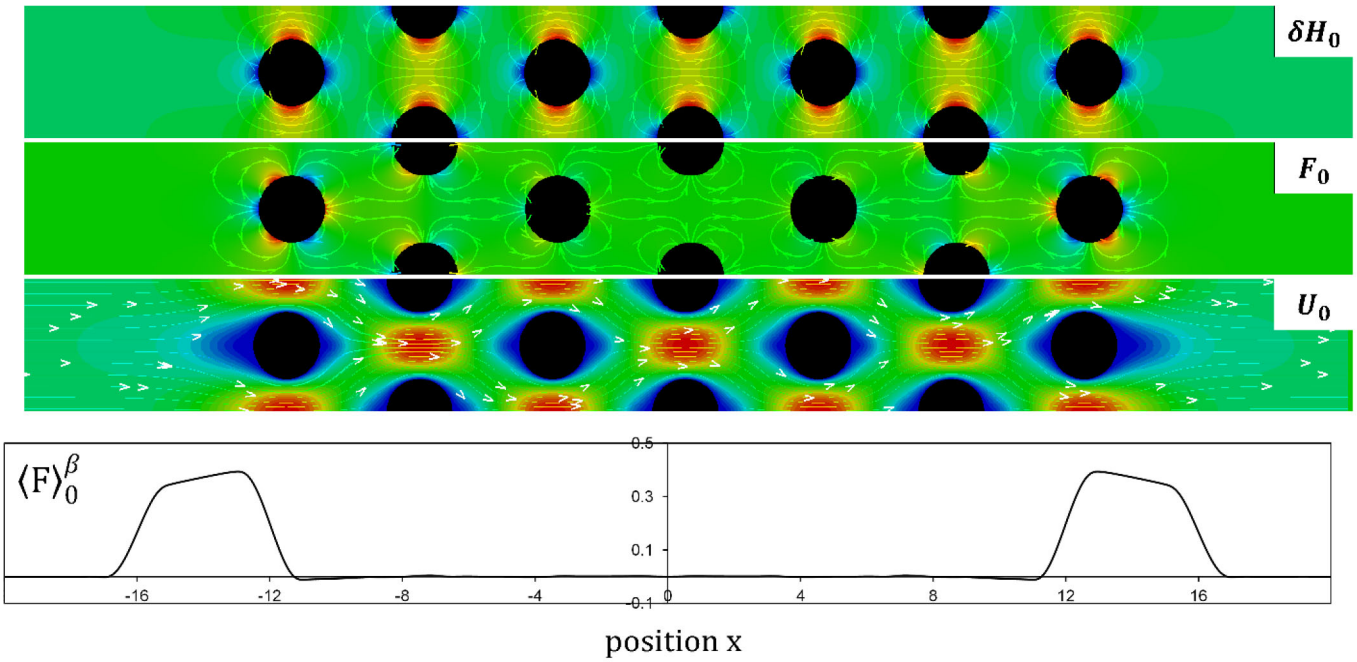

Fig. 9. Shifted arrangement, series of calculations without the influence of advection: Magnetic field perturbation $\delta\mathbf{H}$ (field lines and distribution of $\mathbf{h} \cdot \delta\mathbf{H}$), magnetic force $\mathbf{F}$ (lines of force and distribution of F_x), velocity of the magnetosolutal flow $\mathbf{u}$ (streamlines and distribution of velocity magnitude), plot of averaged magnetic force $\langle \mathbf{F} \rangle^\beta$.

3.2 Shifted arrangement

It is reasonable to verify the general conclusions of the previous section by briefly considering another kind of an ordered porous structure with a different geometry: the shifted arrangement, in which every other cylindrical inclusion is shifted by a half of the period in the vertical direction (fig. 2). The calculations with a different structure of the membrane can give additional evidence that these conclusions are not accidental for a particular geometry but are valid for different kinds of ordered porous structures.

The perturbation of the external magnetic field within the membrane with the shifted arrangement of inclusions is shown in fig. 9. We repeat the general approach used in the previous section comparing two series of simulations without and with account for advection of the ferroparticle concentration (case 0 and case 1 correspondingly).

Imposing a unit concentration gradient the distribution of the magnetic force (1) is calculated (fig. 9). Due to the different geometries the structure of the magnetic force in the bulk of the membrane is significantly different than that in the linear arrangement. In turn the immediate surface of the membrane is geometrically identical for both arrangements. Calculating the cellular average of the magnetic force its magnitude and distribution is similar to the one of the linear arrangement and the same conclusions are valid: the magnetic force still vanishes in the bulk and is concentrated just in the immediate vicinity of the membrane surface.

Next a series of calculations is performed at different porosities without accounting for advection of the ferroparticle concentration (case 0) making use of the predetermined distribution of the magnetic force. The configuration of the flow for this geometry is different from the linear arrangement: the inclusions no longer shadow each other from the flow and there are no stagnant regions between the elements.

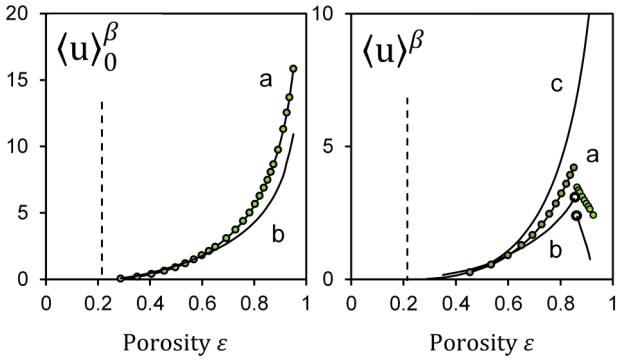

Fig. 10. Shifted arrangement, summary of calculations. Left: calculations without the influence of advection (case 0), dependence of the averaged velocity $\langle u \rangle_0^\beta$ in the bulk of the membrane on porosity: (a) pore-scale simulations, (b) predictions of Darcy's law. Right: dependence of the averaged velocity $\langle u \rangle^\beta$ in the bulk of the membrane on porosity, calculations with account for advection (case 1): (a) pore-scale simulations; (b) predictions of Darcy's law; (c) empirical correlation $\epsilon \langle u \rangle_0^\beta$ where $\langle u \rangle_0^\beta$ is the corresponding velocity calculated from simulations without the influence of advection (case 0).

The velocity $\langle u \rangle_0^\beta$ in the bulk of the membrane is compared with the prediction of Darcy's law (7) in fig. 10.

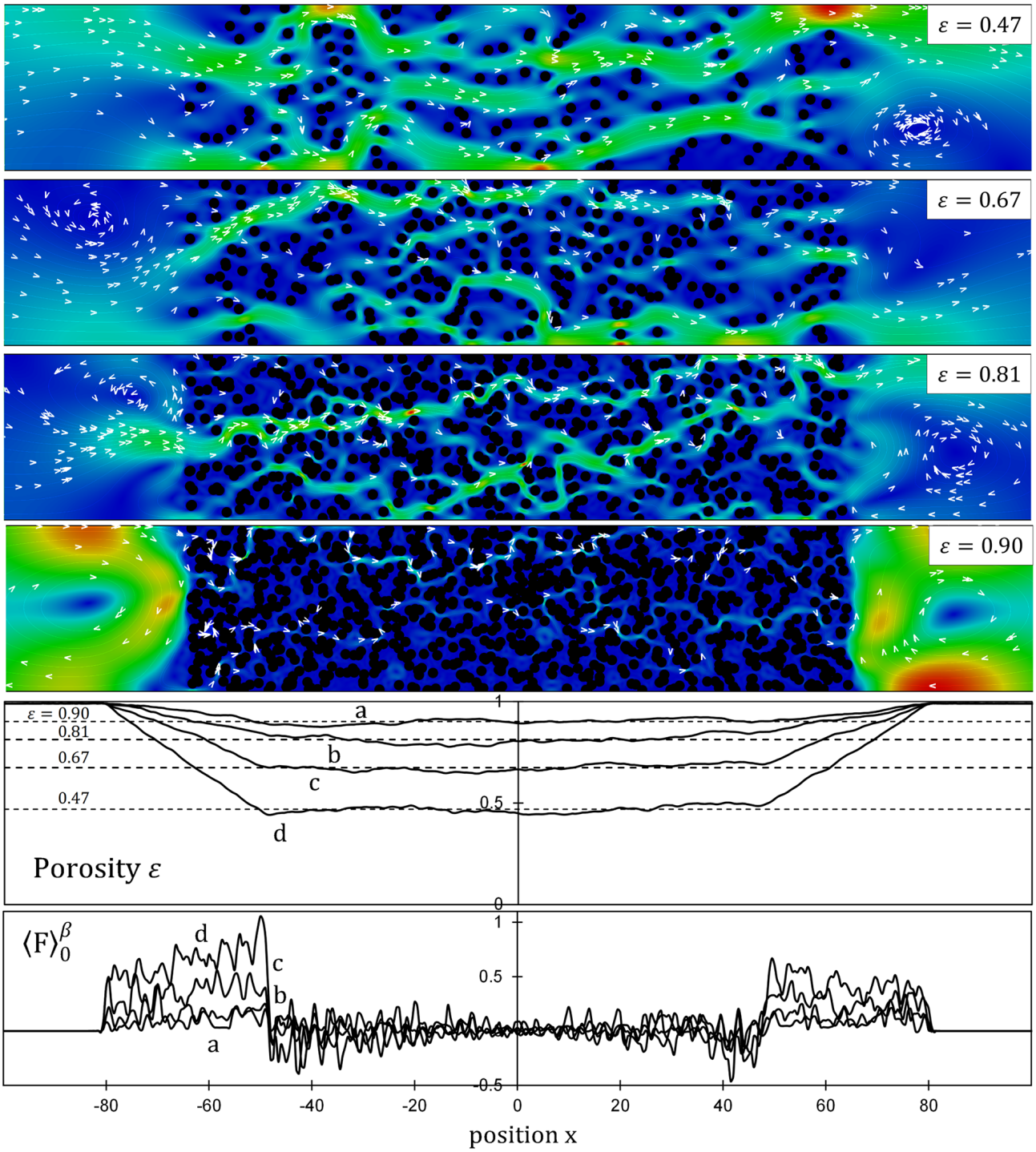

Fig. 11. Disordered porous membranes, series of calculations without the influence of advection: velocity of the magnetosolutal flow **u** (streamlines and distribution of velocity magnitude) in membranes with different porosity (a) $\epsilon \approx 0.90$, (b) $\epsilon \approx 0.81$, (c) $\epsilon \approx 0.67$, (d) $\epsilon \approx 0.47$; plot of porosity ϵ within the membranes, plot of averaged magnetic force $\langle \mathbf{F} \rangle^{\beta}$.

The comparison is slightly better for the shifted arrangement than for the linear arrangement, which was considered in the previous section, but this seems accidental.

In the case 1 simulations with account for advection of the ferroparticles we calculate the gradient of their averaged concentration in the bulk of the membrane. The decrease of the magnitude of the concentration gradient within the membrane is closely proportional to its porosity as in the case of the linear arrangement. Thus this conclusion is not influenced by the particular geometry of the membrane.

The dependence of the averaged flow velocity $\langle u \rangle^{\beta}$ in the center of the membrane on the porosity in the simula-

tions with account for the advective transport is plotted in fig. 10. The velocity grows with increasing the porosity up to a certain threshold. At the value of the porosity $\epsilon \approx 0.87$ the flow velocity starts to decrease further increasing the porosity. While this behavior is similar to the results of the calculations in the linear arrangement the difference is the presence of a discontinuity at the threshold value of the porosity. This discontinuity appears due to the change of the symmetry of the flow through the hydrodynamic instability: at large porosity the flow becomes asymmetric with respect to the midline of the channel. Further increasing the porosity periodic oscillations of the flow can be observed in the simulations.

We note that in the shifted arrangement Darcy's law also fails to correctly describe the velocity in the membrane for the porosity larger than $\epsilon \approx 0.6$. Still, the empirical relation (12) shows acceptable correspondence (fig. 10) in a wide range of the porosity up to the threshold of the instability.

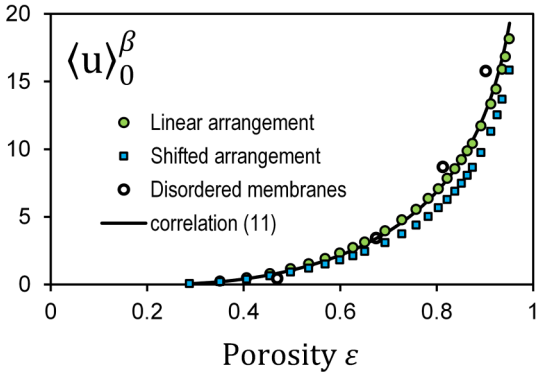

Fig. 12. Summary of calculations without advection of ferroparticle concentration (case 0), comparison of averaged velocity in the bulk of the membrane for all calculated geometric configurations: ordered linear arrangement, ordered shifted arrangement, disordered membrane.

4 Disordered structures

In order to determine whether the periodicity of the ordered porous media that have been considered up to this point plays a significant role in the obtained results we investigate disordered porous structures possessing irregular geometry, for which no unit cell can be defined. For this purpose the systems with a large number of inclusions are necessary to accommodate the large averaging domains for the correct calculation of the distribution of the averaged values [26]. For all calculations the size of the membrane is chosen to be 32×128, which is a compromise between the size of the averaging volume (larger volumes produce lower statistical oscillations of the average quantities, 32×32 is the chosen size), and the numerical complexity of the problem. The structure of the membrane is generated by randomly positioning the cylindrical inclusions with the radius 1 within the domain of this size. The porosity was changed by varying the number of the inclusions composing the membrane. Four cases have been considered with the average porosity (a) $\epsilon \approx 0.90$ (128 inclusions), (b) $\epsilon \approx 0.81$ (256 inclusions), (c) $\epsilon \approx 0.67$ (512 inclusions), (d) $\epsilon \approx 0.47$ (1024 inclusions). The distribution of the porosity within each membrane is illustrated in fig. 11.

Due to the relatively large size of the system for the disordered structures only the calculations with the imposed concentration gradient, *i.e.* without account for advection of the ferroparticle concentration have been performed (case 0). Applying a concentration gradient with a unit magnitude across the membrane the distribution of the magnetic force and the averaged magnetic force can be calculated (fig. 11). Despite the presence of unsmoothed rapid oscillations with respect to the position the magnetic force basically vanishes within the membrane just as was observed previously and with greater clarity in the simulations within the ordered porous structures. The magnetic force is localized in the vicinity of the membrane surface creating a pressure difference driving the magnetosolutal flow through the porous structure.

Making use of the calculated distribution of the magnetic force we calculate the magnetosolutal flow passing through the disordered membrane by solving the Stokes equation (6). The calculated configuration of the flow for all four considered cases of disordered membranes with different porosity is shown in fig. 11. We note that the irregular structure of the membrane surface may cause the appearance of a tangential flow and intensive mixing in the vicinity of the surface, especially at lower values of the membrane porosity, which was not observed in the ordered porous membranes possessing a symmetrical configuration of the membrane surface. Due to the disordered structure of the bulk of the membrane the penetrating flow passes through irregular paths. Decreasing the porosity of the membrane the total magnetosolutal flow also decreases. In the previously considered ordered porous structures this happened just due to the increased shear and the decrease of the Darcy number with the porosity while the number of the percolation paths available to the flow remained the same. In disordered porous structures the number of the percolation paths also decreases with the porosity as evidenced by fig. 11. Then the decrease of the magnetosolutal flow with the decreasing porosity should happen faster in the disordered porous structures than in the ordered ones.

5 Summary

We have performed calculations of the magnetosolutal flow of the ferrocolloid through porous permeable membranes with different structure and porosity. Two series of calculations —with and without account for advection of the ferroparticle concentration— have been performed for the linear and shifted arrangements of inclusions forming the ordered porous structures. An additional series of calculations without account for advection of the ferroparticles has been performed for a random arrangement of inclusions forming disordered porous membranes. We have

shown that regardless the structure of the membrane the magnetic force vanishes within the bulk and remains only in the immediate vicinity of the membrane surface. This surface force creates the pressure difference, which drives the magnetosolutal flow. It is possible that the convective circulations within the individual pores and the resulting pore-scale mixing could lead to the appearance of a negative component of the magnetic force, which opposes the pressure difference originating at the membrane surface. The competition of the bulk and surface forces could lead to instabilities and oscillations of the flow through the membrane at some parameters. Advection of the ferroparticles leads to the decrease of the concentration gradient within the bulk of the membrane as compared to its magnitude in the free stream proportionally to the porosity of the membrane (11). As a consequence the magnetosolutal flow through the membrane is reduced in comparison with its initial magnitude without account for advection of the ferroparticle concentration. This decrease is proportional to the decrease of the concentration gradient in the bulk of the membrane and can be described with acceptable accuracy by a simple empirical correlation (12). This relation holds up to a relatively large value of the porosity $\epsilon \approx 0.87$.

We now plot the summary of the results of our series of calculations without account for advection of the ferroparticle concentration (case 0), *i.e.* the averaged velocity of the magnetosolutal flow in the bulk of the membrane, for all considered configurations of the membrane structure: two ordered arrangements (linear and shifted) and one disordered arrangement of inclusions (fig. 12).

We conclude that the magnitude of the magnetosolutal flow in the permeable membranes weakly depends on the particular geometry of the membrane. The single important geometric parameter is the porosity of the membrane.

Summarizing our finding it is possible to formulate a correlation describing the magnetosolutal flow within the membrane:

$$\epsilon \langle u \rangle^{\beta} = Da\, \mathbf{F}, \tag{13}$$

$$\mathbf{F} = -1.8\epsilon^2(1-\epsilon) Rs_m \nabla \langle c \rangle^{\beta}, \tag{14}$$

In this relation the minus sign shows that the magnetosolutal flow is directed towards decreasing concentration, the term $\epsilon(1-\epsilon)$ comes from the parabolic dependence of $\epsilon Da^{-1} \langle u \rangle_0^{\beta}$ with respect to the porosity, which was discussed previously. The magnitude of the flow is directly proportional to the magnetosolutal Rayleigh number due to the linearity of the Stokes equation. In turn, the contribution $\epsilon \nabla \langle c \rangle^{\beta}$ describes the dependence of the magnetosolutal flow on the gradient of the ferroparticle concentration within the membrane according to (11) and (12).

One of us (Dmitry Zablotsky) acknowledges the support of the European Social Fund, Project 2013/0018/1DP/1.1.1.2.0/13/APIA/VIAA/061.

References

1. E. Blums, A. Mezulis, G. Kronkalns, J. Magn. & Magn. Mater. **169**, 220 (1997).
2. J. Lenglet, A. Bourdon, J. Bacri, G. Demouchy, Phys. Rev. E **65**, 031408 (2002).
3. S. Alves, G. Demouchy, A. Bee, D. Talbot, A. Bourdon, A.M.F. Neto, Philos. Mag. **83**, 2059 (2003).
4. G. Meriguet, G. Demouchy, E. Dubois, R. Perzynski, A. Bourdon, J. Non-Equilib. Thermodyn. **32**, 271 (2007).
5. R. Rosensweig, *Ferrohydrodynamics* (Dover Publications, 2014).
6. E. Blums, J. Magn. & Magn. Mater. **149**, 111 (1995).
7. E. Blums, Magnetohydrodynamics **39**, 369 (2003).
8. M. Maiorov, A. Tsebers, Magnetohydrodynamics **19**, 376 (1983).
9. A. Cebers, M. Igonin, Magnetohydrodynamics **38**, 265 (2002).
10. M. Igonin, Magnetohydrodynamics **40**, 53 (2004).
11. A. Mezulis, E. Blums, Magnetohydrodynamics **40**, 337 (2004).
12. E. Blums, J. Magn. & Magn. Mater. **289**, 246 (2005).
13. D. Zablotsky, E. Blums, Phys. Rev. E **84**, 026319 (2011).
14. D. Zablotsky, E. Blums, Phys. Rev. E **84**, 066305 (2011).
15. D. Zablotsky, A. Mezulis, E. Blums, C.R. Méc. **341**, 449 (2013).
16. T. Volker, S. Odenbach, Phys. Fluids **15**, 2198 (2003).
17. E. Blums, G. Kronkalns, A. Mezulis, V. Sints, J. Magn. & Magn. Mater. **323**, 1334 (2011).
18. E. Blums, A. Mezulis, G. Kronkalns, V. Sints, Magnetohydrodynamics **48**, 451 (2012).
19. E. Blums, V. Sints, G. Kronkalns, A. Mezulis, C.R. Méc. **341**, 348 (2013).
20. E. Blums, V. Sints, A. Mezulis, G. Kronkalns, Magnetohydrodynamics **49**, 360 (2013).
21. H. Davarzani, M. Marcoux, M. Quintard, Int. J. Heat Mass Transfer **53**, 1514 (2010).
22. E. Blums, A. Cebers, M. Maiorov, *Magnetic fluids* (Walter de Gryuter & Co, 1997).
23. D. Griffiths, *Introduction to Electrodynamics*, 3rd edition (Prentice Hall, 2007).
24. E. Blum, Magnetohydrodynamics **15**, 23 (1979).
25. V. Naletova, A. Kvitantsev, J. Magn. & Magn. Mater. **289**, 250 (2005).
26. M. Quintard, S. Whitaker, Chem. Engin. Sci. **48**, 2537 (1993).
27. S. Whitaker, Transport Porous Media **1**, 3 (1986).
28. P. Carman, Trans. Inst. Chem. Engin. **15**, 150 (1937).
29. B. Gebart, J. Composite Mater. **26**, 1100 (1992).
30. M. Quintard, S. Whitaker, Adv. Water Res. **17**, 221 (1994).